1 Mathematical and Computational Background

As discussed in Section **??**, R5 neurons exhibit variety of response properties under different experimental conditions: they show tonic firing during day, $\sim$ 1Hz bursting at night and after sleep deprivation, and low-frequency spiking (potentially mediated by Ca^{2+} channels) following the blockade of Na^{+} channels. The biological mechanisms underlying these responses and the transition between them are poorly understood. This section reviews the background on bursting neurons from mathematical and computational perspectives and concludes with suggestions for modeling the behavior of R5 neurons.

1.1 Models of Bursting Neurons

1.1.1 Preface

As discussed in Section **??**, at the level of ion channels, different ionic mechanisms can underlie bursting, depending on which ionic currents are responsible for initiation and termination of the bursts. However, irrespective of the specific ionic channels involved, resting and spiking states, as well as transitions between them, can exhibit different characteristics across different models. The examples of bursting neurons in Figures **??** and 1 illustrate the case when the resting state is a stable equilibrium and the spiking state is a limit cycle attractor. However, generally, the resting state can also be a limit cycle attractor (not shown here). As the electrophysiological recordings of R5 neurons do not show subthreshold oscillations at the resting state, this case will be omitted in this chapter. The case when the resting state is a stable equilibrium is referred to as ***'point-cycle burster'*** (E. M. Izhikevich 2000), and will be the main focus in the following.

Bursting is commonly modeled as a dynamical system consisting of two - **fast and slow subsystems**, with the fast system having two states - spiking and resting, while the slow system slowly modulates the transition of the fast subsystem between the two states. In other words, modulation of the slow variable causes transitions between the states in the fast subsystem. Mathematically, such transitions can be analyzed using bifurcation theory.

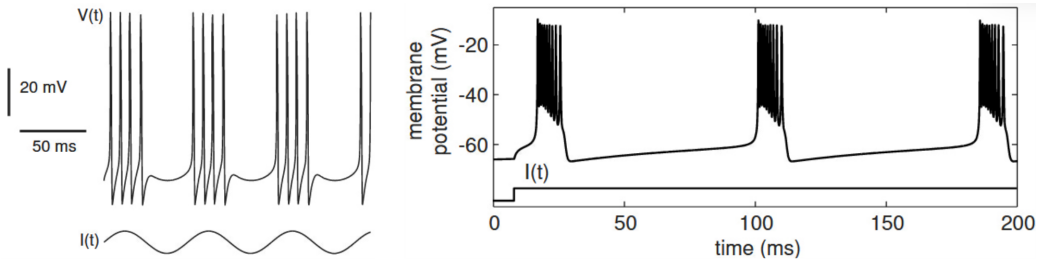

(b) Forced Burster (a) Intrinsic Burster

Figure 1: Forced vs intrinsically bursting neurons. Examples of model neurons bursting due to time-varied external input (a) and intrinsic properties (b). Adapted from (E. M. Izhikevich 2006), with modifications.

1.1.2 Classification

Models of the bursting neurons can be classified according to the modeling approach, response to the external input, or the dynamical characteristics of the transitions between spiking and resting states. The current section provides an overview of these classification frameworks. Classification based on the dynamical characteristics will be discussed in more detail in Section 1.2.

Modeling approach

Based on the modeling approach, they can be classified into **phenomenological** (e.g. proposed by Izhikevich (E. Izhikevich 2003; E. M. Izhikevich 2000), or Hindmarsh-Rose (X.-J. Wang 1993)) and **conductance-based** (first proposed by Hodgkin and Huxley (Hodgkin and Huxley 1952)) models. One of the most widely-used phenomenological models for bursting is the one proposed by Izhikevich (E. Izhikevich 2003), governed by the following system of differential equations:

$$\frac{dv}{dt} = 0.04v^2 + 5v + 140 - u + I \tag{1.1}$$

$$\frac{du}{dt} = a(bv - u) \tag{1.2}$$

where v is the membrane potential, and u represents a recovery variable acting as negative feedback on the membrane potential, accounting for activation of K^+ and inactivation of Na^+ channels, and I represents the external current. The spikes are generated by manually resetting

variables when v reaches predefined threshold v_{thr}:

$$\begin{cases} v \leftarrow c \\ u \leftarrow u + d \end{cases} \quad \text{if } v \geq v_{\text{thr}}$$

By changing the dimensionless parameters a, b, c, and d the model can reproduce a variety of spiking behaviours. However, such phenomenological models are not biologically plausible, as they do not account for the intrinsic mechanisms of activity generation.

On the other hand, conductance-based models describe the interactions between membrane potential and ionic currents, thereby providing insights into the underlying biological mechanisms responsible for observed neuronal activity patterns. Since the aim of this thesis is to understand which biological mechanisms may contribute to the generation of diverse activity patterns observed in R5 neurons, conductance-based models will be the primary focus of the following work.

Furthermore, neurons can be modelled using **single-** or **multicompartment** approaches. In general, the distribution and/or concentration of the ion channels varies across different parts of the neuron, such as soma, dendrites, and axon, with some ion channels expressed in particular regions. In addition, neuronal morphology has been shown to enhance robustness to parameter variations and significantly influence neuronal computations, including synaptic integration, as well as initiation and propagation of action potential. Multicompartment models account for these spatial variations by modeling different neuronal compartments and interactions between them. In contrast, single-compartment models assume a uniform distribution of ion channels and represent neurons as a single, uniform unit. Nevertheless, single-compartment neurons have been found to be sufficient for replicating many experimental observations. Although multicompartment models are more biologically plausible and can better reproduce experimental data, single-compartment neurons are more computationally efficient (see also discussion).

Response to the external input

Generally, any model neuron that spikes can also burst under modulation of time-dependent external input $I(t)$ (E. M. Izhikevich 2006) (***forced burster***, Fig. 1a). However, a neuron can also burst intrinsically under constant input due to the interplay between ionic currents mediated

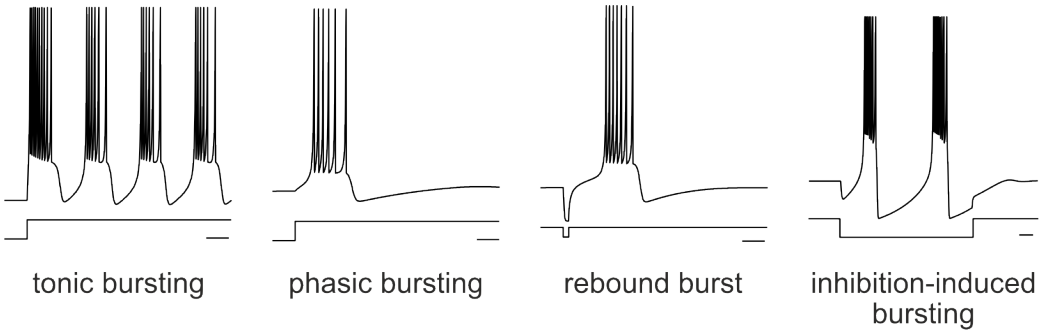

Figure 2: Classification of intrinsically bursting neurons by neuro-computational features. Adapted from (E. M. Izhikevich 2006), with modifications. Electronic version of the figure and reproduction permissions are freely available at `www.izhikevich.com`.

by ion channels present in the membrane of the neuron (***intrinsic burster***, Fig. 1b). Although it is not known whether R5 neurons are intrinsic bursters or not (Raccuglia et al. 2019), as Slow-Wave Activity (SWA) is thought to be generated at the level of R5 (Raccuglia et al. 2019), in the current work, it will be assumed that R5 neurons exhibit bursting behaviour due to intrinsic properties, rather than via time-varied external input (refer to Section **??** for details on the underlying biological motifs).

Bursting in neurons can arise through various mechanisms and is often classified based on the type of external current under which the neuron exhibits bursting behaviour. Models that burst due to a neuron's intrinsic properties can be categorized into one of the following classes: (1) **tonic bursting**, where the neuron generates repetitive bursts in response to a constant depolarizing current, (2) **phasic bursting**, where a single burst followed by a quiescent state is observed near the onset of a constant depolarizing current, (3) **rebound bursting**, where a burst is elicited following termination of hyperpolarizing step current, and (4) **inhibition-induced bursting**, where neuron exhibits periodic bursting during the application of hyperpolarizing external current (E. M. Izhikevich 2006; E. Izhikevich 2004). The examples of each type of bursting are depicted in Figure 2.

Classification based on dynamical characteristics

As it was mentioned in Section 1.1.1, bursting is commonly modelled as an interaction between fast and slow subsystems, with the fast subsystem having two states (spiking and resting), and the slow subsystem governing transition between the two.

Within the framework of a fast-slow system, bursting can be categorized into two classes

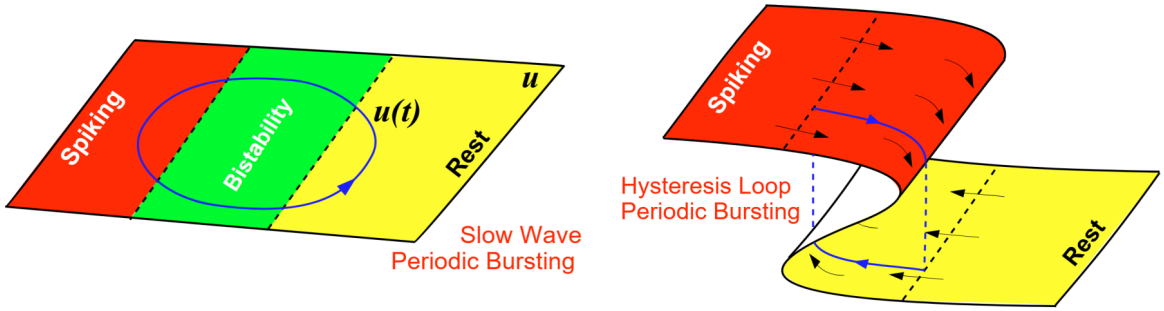

Figure 3: Slow wave and hysteresis-loop bursting. Adapted from (E. M. Izhikevich 2006), with modifications.

depending on the mechanism governing transitions between the two states of the fast subsystem - **hysteresis-loop** and **slow-wave** bursting (Figure 3). One key difference between the two is that slow-wave bursting requires the slow system to be at least 2-dimensional to generate oscillations, whereas the hysteresis-loop bursting can occur with a single slow variable. Additionally, in slow-wave bursting, the transition between spiking and resting states occurs due to reversing the direction of the slow variable (Figure 3, left). In contrast, hysteresis-loop bursting exhibits more complex dynamics - the system remains in a spiking or resting state until the specific threshold is crossed. Reversing the direction of the slow variable is insufficient to induce the transition. This distinguishes the hysteresis loop from slow-wave bursting, where the slow subsystem itself drives periodic transitions between the two states.

It is worth noting that, in case of the slow-wave bursting, according to the textbook-definition (E. M. Izhikevich 2000; E. M. Izhikevich 2006), the slow variable (e.g. u in Equations 1.1-1.2) evolves (relatively) independently of the fast subsystem. However, it does not imply that the slow subsystem is always autonomous, or that it always has a limit-cycle attractor. In some models, feedback from the membrane potential (e.g. E. M. Izhikevich 2006, p. 356) or from variables of the fast subsystem (e.g. E. M. Izhikevich 2000, p. 1201) is required to generate bursting behaviour.

1.2 Bifurcation Analysis

Bifurcation analysis is a powerful tool to investigate the behaviour of a dynamical system. Specifically, how the given system switches between different states when one or multiple parameters (referred to as **bifurcation parameters**) are varied. By definition, bifurcation is a

qualitative change in a system's topological structure that occurs when its parameters cross a bifurcation (or, critical) point (Y. A. Kuznetsov 2023).

Within the framework of the fast-slow subsystems with a single slow variable one can consider the slow variable as a bifurcation parameter and investigate how changing the value of that variable affects the state of the fast subsystem: for what values are the fast subsystem at rest, or spiking state, and how does transition between these states occur. Thus, when the mechanism of bursting is investigated, one can divide the question into two parts: 1) how is the burst initiated?, and 2) how is the burst terminated? In the previous section, cellular mechanisms of these questions were summarized. In the current section, the same questions are approached from the perspective of mathematical analysis. Transition from resting (when the neuron does not fire action potentials) to spiking state is referred to as **bifurcation of equilibria**. Transition from spiking to resting state is referred to as **bifurcation of cycles** (E. M. Izhikevich 2000; E. M. Izhikevich 2006).

Bifurcations are commonly divided into two classes: **local bifurcations** and **global bifurcations** (Zhou 2013). Local bifurcation occurs when the stability of a fixed point is changed when the bifurcation parameter is varied. Here, changes are confined within a small neighbourhood of a single fixed point and can be studied by linear stability analysis. In contrast, changes in the phase space in the case of global bifurcations occur on a larger scale (e.g. when two limit cycles collide with each other) and are harder to detect analytically (Strogatz 2018). Bifurcations may be investigated using analytical methods or semi-analytical numerical tools (such as MATCONT (Dhooge, Govaerts, and Yu. A. Kuznetsov 2003) or AUTO (Doedel et al. 1999)).

1.2.1 Codim-1 bifurcations in planar fast-slow systems

In bifurcation theory, **codimension 1** (or, **codim-1**) bifurcations occur when varying a single bifurcation parameter. If the system has one slow variable, one can study for what values of the slow variable the fast subsystem undergoes a state transition (from resting to spiking state, and vice versa).

Izhikevich studied codim-1 bifurcations in **planar systems**, where the fast subsystem is 2-dimensional (E. M. Izhikevich 2000). He identified 12 relevant codim-1 bifurcations for the resting state, and 10 for the spiking state. For a more detailed overview of the 120 possible

Bifurcation of Equilibria	Frequency	Amplitude
Fold*	nonzero	fixed
Saddle-node on Invariant Cycle (SNIC)**	zero ($\sqrt{\lambda}$)	fixed
Supercritical Hopf	nonzero	zero ($\sqrt{\lambda}$)
Subcritical Hopf	nonzero	arbitrary

Table 1: Bifurcations of Equilibria of Fast Subsystem (adapted from (E. M. Izhikevich 2000) with modifications). *Also called saddle-node

bifurcation pairs, the readers are referred to Table 4 in (E. M. Izhikevich 2000).

As it was discussed in Section 1.1.1, generally, the fast subsystem may or may not exhibit oscillations at the resting state. The system that does not show oscillations at the resting state of the fast subsystem was referred to as a point-circle burster. Out of the above-mentioned 120 bifurcation pairs, 36 exhibit point-circle bursting, out of which 16 can occur in planar systems. The corresponding bifurcations of equilibria and cycles are given in Tables 1 and 2. Each bifurcation type has distinct properties and implications for the system's dynamics. In the following, possible bifurcations for point-circle bursting in planar systems will be summarized. Although the fast subsystem may undergo more than one bifurcation, and the list of possible onset and/or offset bifurcations may extend with increasing dimensionality of the system, investigation of simpler, lower-dimensional systems provides valuable insight into the fundamental mechanisms of bursting. See also Section **??** for the bifurcation analysis of one of the models implemented in this thesis — specifically, the model proposed by Wang (X.-J. Wang 1994).

Bifurcation of Equilibria

Bifurcation of equilibria occurs when the stable fixed point loses its stability. Within the framework of a fast-slow system, the stable fixed point refers to one of the fast subsystems, and the bifurcation happens when the slow variable passes through the critical value. Table 1 summarizes the possible bifurcations of equilibria for point-circle bursting neurons.

Fold (or, **Saddle-Node (SN)**) **bifurcation** occurs when stable and unstable fixed points collide and annihilate each other. The example is illustrated in Figure 4A, which describes the bifurcations of the fast subsystem for one of the bursting neuron models from (Franci, Drion, and Sepulchre 2018). The black line represents the stable (solid) and unstable (dashed) fixed points of the fast subsystem, which depend on the value of the slow variable (here, m_{KCa}). For

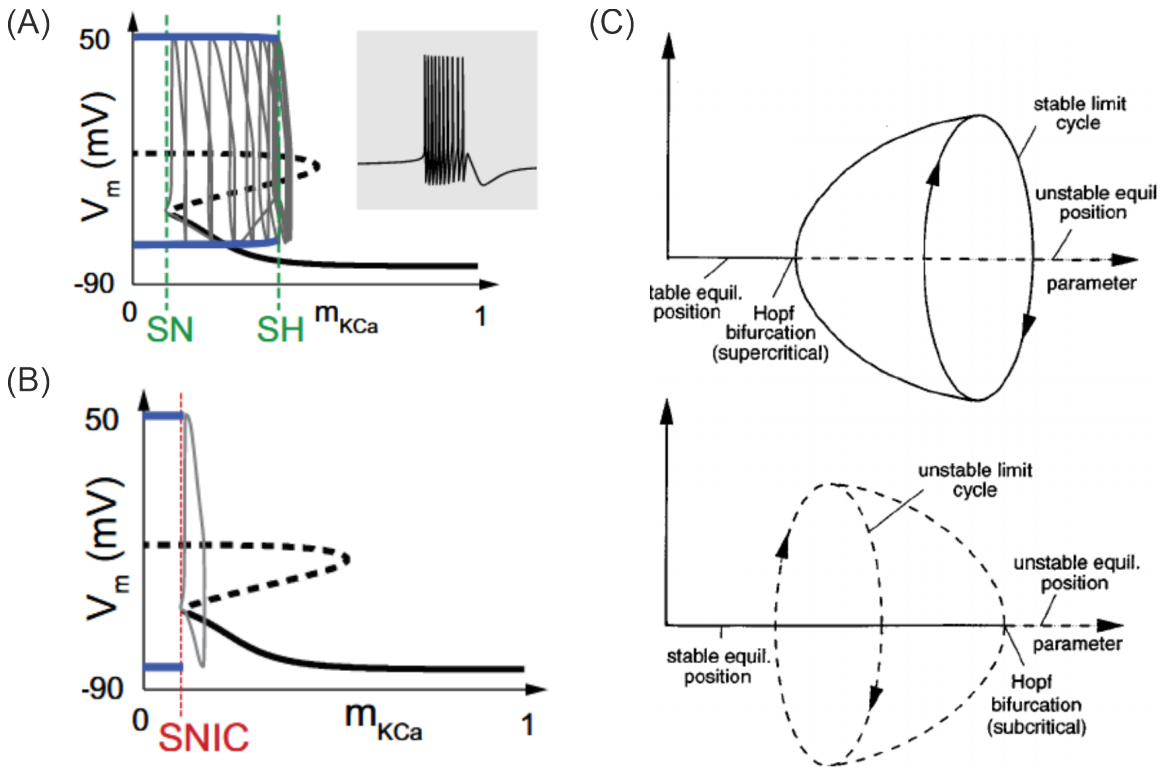

Figure 4: Examples of subcirical Hopf Bifurcation (subHB), SN, Saddle-Homoclinic (SH), and SNIC bifurcations. (A) and (B) adapted from (Franci, Drion, and Sepulchre 2018); (C) adapted with modifications from (Lucero 1999).

large values of m_{KCa}, the fast subsystem is in equilibrium. By reducing the value of the slow variable, two unstable fixed points appear, one of them colliding with the stable fixed point of the fast subsystem (SN). As at that critical point of m_{KCa}, the stable fixed point is annihilated, the trajectory is drawn toward a different attractor of the dynamical system, in this case - stable limit cycle (the solid blue lines indicate the minimal and maximal values of the membrane potential during oscillations).

Saddle-node on Invariant Circle (SNIC) bifurcation, depicted in Figure 4B, is similar to the SN bifurcation. However, here the stable and unstable fixed points lie on a limit cycle. Note, that Figure 4 is intended to illustrate bifurcations of equilibria. Although in the specific example shown in Figure 4B does not exhibit bursting behaviour, bursting can nevertheless arise from a SNIC bifurcation of equilibria in the case of a hysteresis loop (see Figure **??**).

Hopf bifurcation can be classified into two types - **subHB**, and **supercritical Hopf Bifurcation (supHB)**. It occurs when two complex conjugate eigenvalues of the Jacobian matrix cross

the imaginary axis when the bifurcation parameter is varied (note that this implies that the real part of the eigenvalues is zero at the bifurcation point, with opposite signs on either side of the bifurcation). The examples of both types of Hopf bifurcations are illustrated in Figure 4C. In case of supHB, when the stable fixed point loses stability, a stable limit cycle emerges surrounding the unstable fixed point. The oscillations emerge with 0 amplitude and gradually grow in size as the bifurcation parameter moves further from the bifurcation point (Figure 4C top). In contrast, for subHB an unstable limit cycle coexists with a stable fixed point before the bifurcation. As the bifurcation parameter approaches the critical value, the unstable limit cycle collapses into the fixed point, causing it to lose stability. After the bifurcation, similar to SN bifurcation, the trajectory is drawn toward a different attractor of the dynamical system - in the case of bursting models, towards a stable limit cycle.

Note that in the examples above, neither of SN, SNIC, or subHB generates a limit cycle at the bifurcation point. Instead, the limit cycles already exist, and the trajectory is drawn to a preexisting attractor after the fixed point loses stability.

The oscillation of R5 neurons switches from a resting to spiking state with nonzero amplitude. Thus, the underlying bifurcation cannot be of supHB type. On the other hand, for SNIC bifurcation, oscillations emerge with 0 frequency and become faster as the bifurcation parameter moves further from the critical value (see Table 1). However, SNIC bifurcation cannot be ruled out, as it corresponds to the bifurcation of the fast subsystem. The speed of the trajectory in the full system, however, depends on both the fast and slow subsystems.

Bifurcation of Cycles

In two-dimensional systems, the bifurcation of cycles may occur through one of the four mechanisms. They are summarized in Table 2.

One of the possible bifurcations of limit cycles, the **supHB**, has already been discussed in the context of equilibria. The bifurcation mechanism is similar in both cases. In case of bifurcation of cycles, when the bifurcation parameter crosses the critical point, the stable limit cycle collapses into the unstable fixed point, causing it to regain stability. As in the bifurcation of equilibria, the amplitude of the oscillations approaches zero as the bifurcation parameter approaches the critical value.

A limit cycle can also be destroyed by **SNIC** bifurcation. Figure 5A illustrates such a case.

Bifurcation of Cycles	Frequency	Amplitude
SNIC	zero ($\sqrt{\lambda}$)	fixed
Supercritical Hopf	nonzero	zero ($\sqrt{\lambda}$)
Fold Limit Cycle*	nonzero	arbitrary
Saddle Homoclinic Orbit	zero ($1/\lvert \ln \lambda \rvert$)	fixed

Table 2: Bifurcations of Cycles of Fast Subsystem (Adapted from (E. M. Izhikevich 2000) with modifications). *Also called Saddle Node of Limit Cycles.

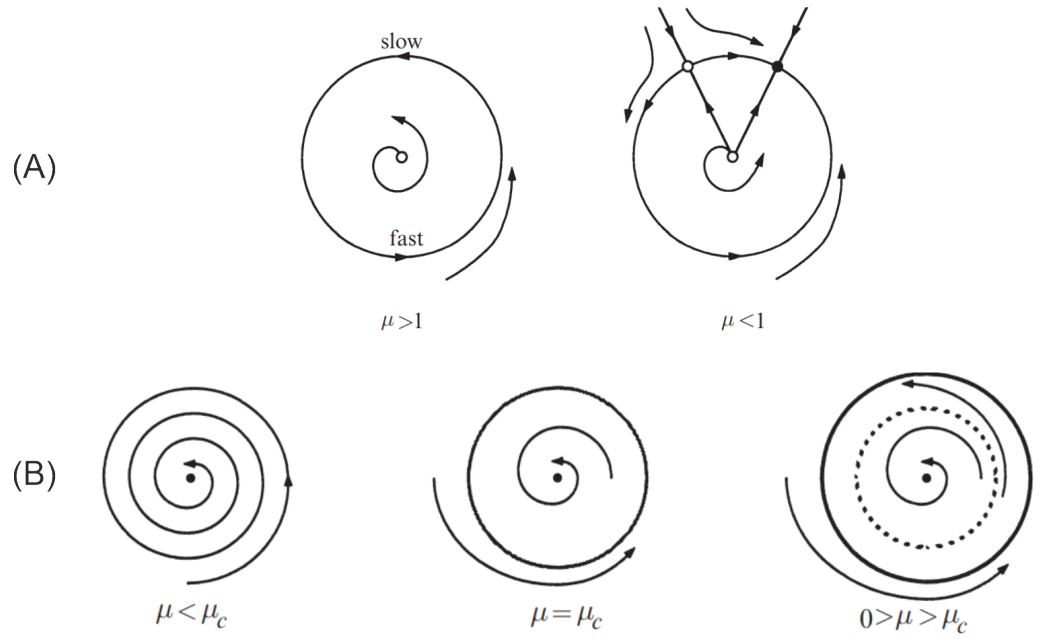

Figure 5: Examples of SNIC and SN bifurcation of cycles. (A) SNIC and (B) SN bifurcations of cycles. Adapted from (Strogatz 2018) with modifications.

Here, when the bifurcation parameter (μ) approaches 1 from the positive side, the system exhibits a bottleneck behaviour - trajectory slows down near the top region of the limit cycle and the period becomes infinite at critical point ($\mu = 1$) when a fixed point appears on the limit cycle. When μ is decreased further, the fixed point splits into stable and unstable fixed points (left). Note that the fixed points here correspond to equilibria of the fast subsystem. In the absence of the slow subsystem, the trajectory would have converged to a stable fixed point. However, the fixed point is not necessarily stable in the system. Thus, after the SNIC bifurcation, the trajectory may instead follow the stable manifold of nodes corresponding to the resting state of the fast subsystem.

The third mechanism is called **fold bifurcation**, or **SN bifurcation of cycles**. An example

is shown in Figure 5B. In this scenario, when the bifurcation parameter (μ) is larger than the critical value (μ_c, right plot in Figure 5), stable and unstable limit cycles coexist together with a stable fixed point. At the bifurcation point, the two cycles collide with each other, resulting in the birth of a half-stable cycle. Trajectories that lie outside the half-stable cycle are drawn towards it, whereas those within the cycle are drawn towards the stable fixed point (middle plot in Figure 5). When μ is decreased further, the limit cycle disappears, leaving the fixed point as the only stable attractor of the system (left plot in Figure 5).

Finally, a stable limit cycle may collide with the saddle point, creating a homoclinic orbit. Example of SN and homoclinic bifurcations of cycles will be illustrated in Section **??**.

1.3 Conductance Based Models: Beyond Two Timescales

The previous section was based on the assumption that the dynamics can be decomposed into fast and slow timescales. However, this is not always the case.

First, if the timescale separation of the two subsystems is not large enough (Ihikevich proposed the difference in the factor of ~ 0.1 (E. M. Izhikevich 2006; E. M. Izhikevich 2006)), then the fast-slow decomposition might not be suitable to describe the dynamics. Second, if the system has more than one slow variable, investigation of the dynamics is not as straightforward, although methods have been proposed to aggregate variables having similar timescales (Franci, Drion, and Sepulchre 2014).

Various models have been introduced to model this or that neuronal activity using multiple timescales (Fazli, Vo, and Bertram 2020; Franci, Drion, and Sepulchre 2018). Notably, one of these studies highlighted the importance of a third timescale operating between the fast and slow subsystems (Franci, Drion, and Sepulchre 2018). In this framework, the authors classify the slow variable discussed above as "ultraslow" and refer to the additional variable with an intermediate timescale as "slow". The authors report that incorporating depolarizing current with slow activation or hyperpolarizing current with slow inactivation makes the model robust to parameter variations. Thus, reducing the dimensionality of the system by treating such variables as instantaneous may reduce the robustness of the model to parameter variations.

Finally, not every model can be decomposed into fast and slow subsystems. Instead of a slow variable modulating the state transitions of the fast subsystem, the trajectory might follow

a curved manifold that resembles bursting dynamics. This type of attractor is commonly referred to as Hedgehog limit cycle (E. M. Izhikevich 2000).

1.4 Modeling Ion Channels

As it was discussed in section **??**, the magnitude of the current that flows through an ion channel may depend on membrane potential, extracellular and intracellular ion concentrations, and/or temperature. This section summarizes the mathematical background for modeling ion channels.

1.4.1 Ohmic vs Goldman-Hodgkin-Katz (GHK) current

The current through an ion channel can be modelled using either Ohm's law or GHK current equation. Ohmic current assumes a linear relationship between voltage and conductance (see e.g. (Huguenard and McCormick 1992; Amarillo et al. 2014)):

$$I_c(V,t) = g_c(V,[\text{ion}]_\text{i},t)(V - V_c) \tag{1.3}$$

where V is membrane potential, $g_c(V,[\text{ion}]_\text{i},t)$ is conductance which is a function of membrane potential V, intracellular ion concentration $[\text{ion}]_\text{i}$ and time t (modeling g_c will be discussed in Section 1.4.2), V_c is reversal potential. Here, the concentration difference between the extracellular and intracellular ion concentrations is hidden inside V_c (see Equation **??** in Section **??** for the case when an ion channel is permeable to one ion). GHK equation, on the other hand, models a nonlinear relationship between the variables in explicit way (see e.g. (Huguenard and McCormick 1992; Destexhe, Neubig, et al. 1998)):

$$I_c(V,t) = g_c(V,t)Pz^2\frac{VF^2}{RT}\frac{[\text{ion}]_\text{i} - [\text{ion}]_\text{o}\exp\left[-zFV/(RT)\right]}{1-\exp\left[-zFV/(RT)\right]} \tag{1.4}$$

where, P is permeability, R is the universal gas constant, T is temperature measured in Kelvin, F is Faraday's constant, z is the valence of the ion, whereas $[\text{Ion}]_\text{in}$ and $[\text{Ion}]_\text{o}$ are ion concentrations inside and outside membrane. **Note:** Units of the parameters and variables are not specified here, as they may vary across different models. For the specific values and units used in the models

implemented in this thesis, **??**.

Equation **??** for the reversal potential can be obtained from 1.4 if one considers the equilibrium condition, where the ionic current $I_c = 0$. Nernst's equation assumes that ion concentrations are fixed. However, Equation 1.3 can still be used when ion concentration dynamics are incorporated in the model by recalculating the reversal potential at each stimulation step.

For some ion channels, Equation 1.3 is sufficient to reproduce experimentally obtained voltage-current relationships. However, for other channels Ohmic current does not provide good estimates and GHK current equation should be used to obtain better fit between experimental data and simulations (Huguenard and McCormick 1992) (see also Section **??** on modeling *Drosophila* T-type Ca^{2+} ion channels).

1.4.2 Modeling conductance: activation and inactivation gates

In the previous section, $g_c(V, [\text{ion}]_\text{i}, t)$ was introduced to represent the conductance of a given ion channel. This function captures the gating mechanism, specifically. activation and inactivation gates - described in Section **??**. g_c is generally governed by the following equation:

$$g_c(V, [\text{ion}]_\text{i}, t) = \overline{g_c} m^p h^q \tag{1.5}$$

Here, $\overline{g_c}$ denotes the maximal conductance of the channel, $m = m(V, [\text{ion}]_\text{i}, t)$ and $h = h(V, [\text{ion}]_\text{i}, t)$ represent the activation and inactivation gating variables, respectively. The exponents p and q correspond to the number of activation and inactivation gates, respectively. m (h) represents the fraction of gates for which one of the p (q) gates is in the open state. Note that for a given ion channel, all gates should be in the open state for the current to pass through it. For leak channels, which lack both gating mechanisms, $p = q = 0$.

Kinetics of activation and inactivation variables can be described by the following differential equation (X. J. Wang, Rinzel, and Rogawski 1991):

$$\frac{dx}{dt} = \alpha_x(1 - x) - \beta_x x \tag{1.6}$$

where $x \in [0, 1]$ is a placeholder for the gating variables m or h; α_x and β_x are transition rates between open and close states (Figure 6). The rates may depend on voltage and/or the

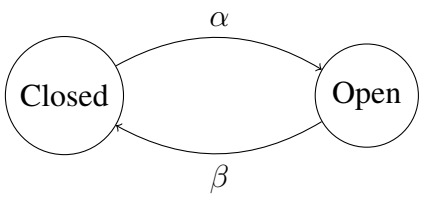

Figure 6: Transition diagram for the first-order kinetic model of gating variables

intracellular concentration of a specific ion. Equation 1.6 can be rewritten as

$$\frac{dx}{dt} = \frac{x - x_\infty}{\tau_x} \tag{1.7}$$

where $x_\infty = \alpha_x/(\alpha_x + \beta_x)$, and $\tau_x = 1/(\alpha_x + \beta_x)$. x_∞ is commonly referred to as **steady state activation**, and h_∞ - steady state inactivation functions. τ_x $x \in m, h$ are corresponding **time constants**. In equations 1.6 and 1.7 dependency of variables on voltage, time and intracellular ion concentration has been omitted for clarity.

The functions for x_∞ and τ_x, as well as exponents p and q are generally derived from voltage-clamp recordings, while the maximal conductance is typically chosen to fit the model output to the experimental data (see Section **??** for the modeling of T-type Ca^{2+} channels).

Equation 1.7 is sometimes written as

$$\frac{dx}{dt} = \phi_x \frac{x - x_\infty}{\tau_x} \tag{1.8}$$

to account for the temperature factor. ϕ_x is called $Q10$ value and is defined as (Sterratt 2015):

$$\phi_x = \frac{\text{Rate of process at temperature } T + 10°\text{C}}{\text{Rate of process at temperature } T} \tag{1.9}$$

The equations 1.6 and 1.7 describe first-order kinetics, with one open and one closed state. However, to account for more complex gating behaviour, higher-order kinetics have been proposed that incorporate multiple open and/or closed states and diverse transition pathways between them (see e.g. (X. J. Wang, Rinzel, and Rogawski 1991; Bruno, Yang, and Pearson 2005)).

Finally, Equation 1.5 assumes that, in the case of multiple activation and/or inactivation

gates, they exhibit similar kinetics (reflected in the use of the exponents p and q). However, some studies have proposed models in which different gates are characterized by different time constants to capture more complex dynamics (see e.g. (Destexhe and Babloyantz 1993)).

1.5 Oscillations after TTX Application

As shown Section **??**, after Na channels were blocked R5 neurons exhibited slow oscillations likely mediated by Ca^{2+} channels. The width of the spikes (~ 100ms) was observed to be considerably smaller than interspike intervals (~ 2s). Such dynamics may arise through one of the following mechanisms: during the interspike interval

1. the trajectory may pass near the bifurcation of equilibria (Hopf of SNIC), where time derivatives of all variables are close to 0, or

2. the system consists of fast and slow subsystems, and the trajectory evolves along the slow manifold, where the fast subsystem is at equilibria while the slow subsystem gradually drives the system toward the spiking threshold.

Such slow oscillations have been reported when the trajectory passes near a Hopf bifurcation (Doi and Kumagai 2005). However, the authors showed that the oscillation period depends exponentially on the injected current. Such behaviour is expected, as such dynamics require a specific intersection of the nullclines, and a slight deviation may significantly affect the dynamics. Similarly, near SNIC bifurcation the oscillation period varies as $\sqrt{\lambda}$, where λ is the distance from the bifurcation (Strogatz 2018; E. M. Izhikevich 2000) (see also Table 1). In both cases, slight variations in the external input can cause large changes in the oscillation period. However, such large variations in the oscillation period were not observed in the experiments. This suggests that in order to exhibit robustness to noise and small parameter variations, the system likely involves a slow variable operating on an ultra-slow timescale (order of seconds).

Apart from slow oscillations, the spikes after blockade of Na^+ channels showed apparent afterhyperpolarization (AHP) (see Sections **??** and **??**). Such undershoots of the membrane potential below the quasi-resting state have been associated with the h-current, mediated by Hyperpolarization-activated Cyclic Nucleotide-gated (HCN) channels (Oswald et al. 2009; Bonin et al. 2013). However, the presence of these channels is not a necessary condition for

AHP. As depicted in Figure 7, the presence of undershoot depends on the location of the two attractors of the dynamical system - the limit cycle and (quasi) stable equilibrium.

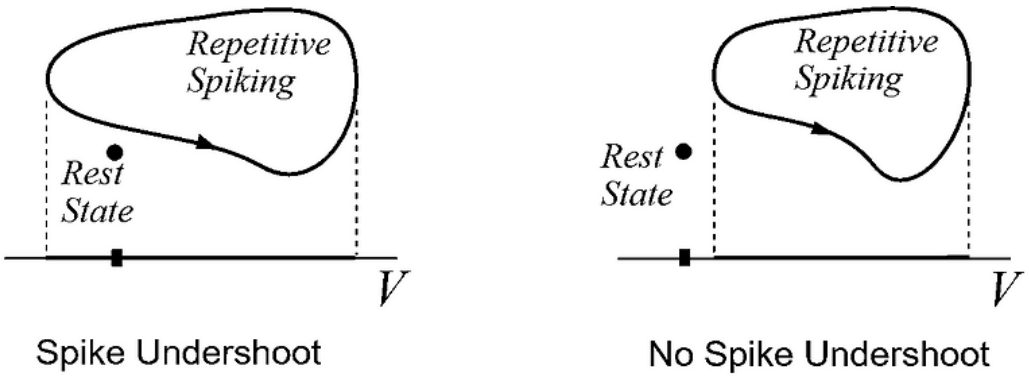

Figure 7: Projection of the limit cycle and resting state on the voltage axis. The spike undershoot depends on the location of the limit cycle attractor and (quasi) stable equilibrium of the dynamical system. Adapted from (E. M. Izhikevich 2000), with modifications.